

OPTIMAL PRESSURE BOUNDARY CONTROL OF STEADY FLUID STRUCTURE INTERACTION SYSTEMS

ANDREA CHIERICI¹, LEONARDO CHIRCO^{1*}, ROBERTO DA VIÀ¹,
PIETRO MACCARI AND SANDRO MANSERVISI¹

¹ University of Bologna - Department of Industrial Engineering
Via dei Colli 16, Laboratory of Montecuccolino - DIN
e-mail: leonardo.chirco2@unibo.it

Key words: Optimal Boundary Control, Adjoint Control, Fluid-Structure Interaction.

Abstract. In the last years adjoint optimal control has been increasingly used for design and simulations in several research fields such as shape optimization problems, fluid-solid conjugate heat transfer and turbulent flows. Recently the study of Fluid-Structure Interaction problems and its control have gained popularity because of many interesting applications in engineering and biomedical fields. Fluid-structure interaction systems consist of one or more solid structures that deform by interacting with a surrounding fluid flow. FSI simulations evaluate the tensional state of the solid component and take into account the effects of the deformations on the motion of the interior fluids. In many engineering applications it is interesting to study the inverse FSI problem which aims to achieve a certain objective by changing some design parameters such as forces, boundary conditions or geometrical domain shapes. In this paper we would like to study these inverse FSI problems by using an optimal control approach based on Lagrangian multipliers and adjoint variables. In particular we propose a pressure boundary optimal control method with the purpose to control the solid behavior by changing the fluid pressure on a domain boundary. The optimality system is derived from the first order optimality condition by taking the Fréchet derivatives of the Lagrangian with respect to all the variables involved. This system is solved by using and comparing different line search methods with a finite element code with mesh-moving capabilities for the study of large solid displacements. In order to support the proposed approach we perform numerical tests where the fluid domain boundary pressure controls the displacement that occurs in a well defined region of the solid domain. The approach presented in this work is general and can be used to assess different objectives and complex geometries.

1 INTRODUCTION

In Fluid-Structure Interaction (FSI) problems the fluid flow changes the tensional state of a solid structure that is left free to move and the solid deformation has an important effect on the fluid flow. Examples of this type of systems are quite common in engineering, like wind turbines, man-made drones and in the study of biological systems such

as hemodynamics. In literature these topics are investigated deeply and the interested reader can see [1, 2, 3, 4, 5, 6, 7, 8, 9]. Optimization has always been used to improve the performance of engineering devices. Nowadays several approaches to optimization are available, such as single and multi-objective, adjoint or sensitivity based methods, evolutionary algorithms and many others. In literature there are several works dealing with this subject, for a quick review the interested reader can see [10, 11, 12, 13, 14, 15] and references therein. Many attempts to apply optimization techniques to FSI problems can be found in literature, for example one can see [16] where the authors propose a solution method for the problem of optimizing a non-linear aeroelasticity system in a steady-state flow by using a sensitivity method. The work in [17] deals with general shape optimization methods based on design sensitivity analysis.

In this work we refer to adjoint based methods, which have been proven to be a good approach for the optimal control of complex problems in which Computational Fluid Dynamics simulations can be performed on the system of interest, see for example [16, 17]. Moreover these methods have a solid mathematical background and the existence of local optimal solutions can be proven for many interesting cases, [17, 18]. We are interested in a monolithic approach to the solution of the FSI system leading to a stable and well defined solution in a finite element setting [19, 20]. Inside this framework we study a pressure boundary optimal control problem applied to the monolithic FSI system. The objective of the control is the matching of a displacement field in a particular region of the solid domain. This is accomplished by changing the pressure on the fluid inlet boundary which alters the fluid flow profile and thus deforms the shape. The optimality system which consists of the state, the adjoint system and the control equation is derived directly from the minimization problem. Since solving iteratively the optimality system with a steepest descent method shows slow convergence we propose a quasi-Newton method to improve the algorithm, see [11]. We report some numerical results obtained by the implementation of the optimal control algorithm in a finite element parallel code designed for multiphysics simulations.

2 MATHEMATICAL MODEL

In this section we first describe the mathematical formulation of the steady-state FSI problem, then we derive the optimality system that arises from the Lagrangian minimization and finally we present the algorithm used to solve it.

We now introduce the notation used for functional spaces in this paper, for a detailed description see [21, 22]. On Ω we denote with $L^2(\Omega)$ the space of square integrable functions and with $H^s(\Omega)$ the standard Sobolev space with norm $\|\cdot\|_s$ ($H^0(\Omega) = L^2(\Omega)$ and $\|\cdot\|_0 = \|\cdot\|$). Let $H_0^s(\Omega)$ be the space of all functions in $H^s(\Omega)$ that vanish on the boundary of Ω and $H^{-s}(\Omega)$ the dual space of $H_0^s(\Omega)$. The trace space for the functions in $H^1(\Omega)$ is denoted by $H^{1/2}(\Gamma)$.

Let us consider a bounded open set $\Omega \subset \mathbb{R}^n$ which is split into a structure domain Ω_s and a fluid domain Ω_f , so that $\Omega = \Omega_s \cup \Omega_f$ and $\Omega_s \cap \Omega_f = \emptyset$. We denote with $\Gamma = \partial\Omega$ the outer boundary, which is then split into $\Gamma_s = \Gamma \cap \partial\Omega_s$ and $\Gamma_f = \Gamma \cap \partial\Omega_f$, the solid and fluid boundary, respectively. The surface $\Gamma_i = \partial\Omega_s \cap \partial\Omega_f$ shared between the solid and

the fluid is the *fluid-structure interface*. The system of equations governing our steady state FSI problem is the following

$$\nabla \cdot \mathbf{v}_f = 0 \quad \text{on } \Omega_f, \quad (1)$$

$$\rho_f(\mathbf{v}_f \cdot \nabla)\mathbf{v}_f - \nabla \cdot \sigma_f = 0 \quad \text{on } \Omega_f, \quad (2)$$

$$\nabla \cdot \sigma_s(\mathbf{l}_s) = 0 \quad \text{on } \Omega_s, \quad (3)$$

where \mathbf{l} is called *displacement field*, \mathbf{v}_f and ρ_f are the fluid velocity and density, respectively. We consider the interaction of a viscous incompressible Newtonian fluid obeying to the Navier-Stokes equations with an hyperelastic compressible St. Venant Kirchhoff material. Then the fluid stress tensor σ_f and the solid Cauchy strain tensor σ_s read

$$\sigma_f(p_f, \mathbf{v}_f) := -p_f \mathbf{I} + \mu_f(\nabla \mathbf{v}_f + \nabla \mathbf{v}_f^T), \quad (4)$$

$$\sigma_s(\mathbf{l}_s) := \lambda_s(\nabla \cdot \mathbf{l}_s)\mathbf{I} + \mu_s \nabla \mathbf{l}_s, \quad (5)$$

where p_f is the fluid pressure, μ_f the dynamic viscosity of the fluid while λ_s and μ_s are the solid Lamé parameters. The unknown fields of the strong FSI system are $(\mathbf{v}_f, p_f, \mathbf{l}_s, \mathbf{l}_f)$, with the solid displacement \mathbf{l}_s being solution of the elasticity equation (3). Therefore the deformed solid domain $\Omega_s(\mathbf{l}_s)$ is expressed as

$$\Omega_s(\mathbf{l}_s) = \{\mathbf{x} \in R^3 \mid \mathbf{x} = \mathbf{x}_0 + \mathbf{l}_s\}, \quad (6)$$

where the vector \mathbf{x}_0 defines the initial solid domain position. On the other hand, \mathbf{l}_f is an artificial fluid deformation field defined as an arbitrary extension operator over the fluid domain Ω_f , see [3].

The strong FSI formulation has to be closed with the following boundary and interface conditions

$$\begin{aligned} \mathbf{v}_f &= \mathbf{v}_0 && \text{on } \Gamma_{fd}, \\ \mathbf{l}_s &= \mathbf{l}_0 && \text{on } \Gamma_{sd}, \\ \sigma_f \cdot \mathbf{n} &= 0 && \text{on } \Gamma_{fn}, \\ \sigma_s \cdot \mathbf{n} &= 0 && \text{on } \Gamma_{sn}, \\ \sigma_f \cdot \mathbf{n} &= \sigma_s \cdot \mathbf{n} && \text{on } \Gamma_i, \\ \mathbf{v}_f &= 0 && \text{on } \Gamma_i, \end{aligned} \quad (7)$$

where on Γ_{fd} and Γ_{sd} we impose Dirichlet boundary conditions, while on Γ_{fn} and Γ_{sn} standard homogeneous outflow boundary conditions are imposed for the displacement and velocity fields. On the interface Γ_i we have that the fluid velocity has to vanish and the normal components of the stress tensors σ have to be continuous. By solving the FSI system with a monolithic approach, where the same solver is used for both the fluid and solid sub-domains, the coupling conditions at the interface (7) are automatically satisfied. Conversely the use of a *segregated* approach allows to solve the fluid and solid sub-problems with already existing dedicated solvers, but the interface coupling conditions have to be imposed iteratively.

2.1 The optimality system

In this work we study a solid deformation matching problem, where the control variable is the pressure on a fluid boundary $\Gamma_c \subset \Gamma_f$. In an optimal control framework it is of great importance the definition of the *cost* or *objective* functional that one aims to minimize.

$$\mathcal{J}(\mathbf{l}_s, p_c) = \frac{1}{2} \int_{\Omega_d} \|\mathbf{l}_s - \mathbf{l}_d\|^2 d\Omega + \frac{1}{2} \beta \int_{\Gamma_c} \|p_c\|^2 d\Gamma. \quad (8)$$

Here the first term takes into account the distance in norm of the solid displacement \mathbf{l}_s from a target deformation value \mathbf{l}_d over the solid sub-domain $\Omega_d \subseteq \Omega_s$. The functional is completed with a regularization term needed to penalize p_c , thus obtaining a boundary pressure in the space of square integrable functions $L^2(\Omega)$. If a too high value of β is chosen the control becomes too smooth and the objective cannot be achieved well, while a lack of regularization leads to convergence issues in the numerical solution of the problem.

To obtain the optimality system we write the full constrained Lagrangian of the problem which is composed of the cost functional and state equations multiplied by the appropriate Lagrangian multipliers

$$\begin{aligned} \mathcal{L}(p_f, \mathbf{v}_f, \mathbf{l}_s, \widehat{\mathbf{l}}_s, p_a, \mathbf{v}_a, \widehat{\mathbf{l}}_a, \widehat{\mathbf{s}}_a, \beta_a) &= \mathcal{J}(\mathbf{l}_s, p_c) + \int_{\Omega_f} (\nabla \cdot \mathbf{v}) p_a d\Omega + \int_{\Omega_s} (\nabla \cdot \mathbf{v}) p_a d\Omega \\ &+ \int_{\Gamma_c} (\mathbf{v}_a \cdot \mathbf{n}) p d\Gamma + \int_{\Omega_f} [\rho_f (\mathbf{v} \cdot \nabla) \mathbf{v} + \nabla p - \nabla \cdot (\mu_f \nabla \mathbf{v})] \cdot \mathbf{v}_a d\Omega \\ &+ \int_{\Omega_s} \nabla \cdot [\mu_s \nabla \mathbf{l} - \nabla p] \cdot \mathbf{v}_a d\Omega + \int_{\Omega_s} \nabla^2 \mathbf{l} \cdot \widehat{\mathbf{l}}_a d\Omega \\ &+ \int_{\Gamma_i} \widehat{\mathbf{s}}_a \cdot \left[(\widehat{\mathbf{l}}_s - \mathbf{l}_s) + \frac{\mathbf{v}}{h} \right] d\Gamma + \int_{\Omega_s} \beta_a \cdot \left[\mathbf{v} - h(\mathbf{l}_s - \widehat{\mathbf{l}}_s) \right] d\Omega. \end{aligned} \quad (9)$$

In (9) we have introduced the auxiliary mesh displacement $\widehat{\mathbf{l}}_s$, defined only over the solid domain and solution of a Laplace operator. The velocity field \mathbf{v} has been extended to the whole domain Ω as

$$\mathbf{v} = \begin{cases} h(\mathbf{l}_s - \widehat{\mathbf{l}}_s) & \text{on } \Omega_s, \\ \mathbf{v}_f & \text{solution of (1)-(2) on } \Omega_f, \end{cases} \quad (10)$$

with h being a positive constant. It is clear that at steady state conditions $\Omega_s(\mathbf{l}_s) = \Omega_s(\widehat{\mathbf{l}}_s)$, with $\mathbf{v}_s = 0$ in the solid. By taking the Fréchet derivatives of the Lagrangian with respect to the adjoint variables the weak form of the state system (1-3) is obtained, together with the correct boundary and interface conditions. When the derivatives are taken with respect to the state variables, after some term rearrangement, the adjoint system in weak

form reads

$$\int_{\Gamma_c} (p_c \beta + \mathbf{v}_a \cdot \mathbf{n}) \delta p \, d\Gamma - \int_{\Omega_f} (\nabla \cdot \mathbf{v}_a) \delta p \, d\Omega - \int_{\Omega_s} (\nabla \cdot \mathbf{v}_a) \delta p \, d\Omega = 0 \quad \forall \delta p \in L^2(\Omega), \quad (11)$$

$$\int_{\Omega_f} [\rho_f (\delta \mathbf{v} \cdot \nabla) \mathbf{v} \cdot \mathbf{v}_a + \rho_f (\mathbf{v} \cdot \nabla) \delta \mathbf{v} \cdot \mathbf{v}_a + \mu_f \nabla \delta \mathbf{v} : \nabla \mathbf{v}_a] \, d\Omega + \int_{\Omega_f} (\nabla \cdot \delta \mathbf{v}) p_a \, d\Omega + \quad (12)$$

$$\int_{\Omega_s} [\mu_s \nabla \delta \mathbf{v} : \nabla \mathbf{v}_a] \, d\Omega + \int_{\Omega_s} (\nabla \cdot \delta \mathbf{v}) p_a \, d\Omega + \int_{\Omega_d} w (\mathbf{1}_s - \mathbf{1}_d) \delta \mathbf{v} \, d\Omega = 0 \quad \forall \delta \mathbf{v} \in H_{\Gamma_{fd} \cup \Gamma_{sd}}^1(\Omega).$$

The shape derivatives with respect to the fluid and solid domain have been taken into account and simplified. Since Ω_d and Γ_c are fixed and the system is solved by using a monolithic approach, then the shape derivative contributions appear only in the equation for the adjoint displacement \mathbf{l}_a . We do not need the solution of the \mathbf{l}_a adjoint equation to compute the pressure boundary control p_c and therefore it may be neglected.

Finally, when considering the surface terms in (11) we obtain the following gradient equation for the control pressure p_c on the controlled surface Γ_c

$$p_c = p = -\frac{\mathbf{v}_a \cdot \mathbf{n}}{\beta}. \quad (13)$$

In order to recover the strong form of the *adjoint system* it is necessary to perform integration by parts on the terms where the variations of the state variables are differentiated. After performing the integration by parts, we recover the adjoint state $(\mathbf{v}_a^f, \mathbf{v}_a^s, p_a) \in \mathbf{H}_{\partial\Omega^f - \Gamma_i}^1(\Omega^f) \cap \mathbf{H}^2(\Omega^f) \times \mathbf{H}_{\partial\Omega^s - \Gamma_i}^1(\Omega^s) \cap \mathbf{H}^2(\Omega^s) \times L_0^2(\Omega^f) \cap \mathbf{H}^1(\Omega^f)$, by solving

$$\nabla \cdot \mathbf{v}_a^f = 0, \quad (14)$$

$$-\rho_f (\nabla \mathbf{v})^T \mathbf{v}_a^f + \rho_f [(\mathbf{v} \cdot \nabla) \mathbf{v}_a^f] + \nabla p_a - \nabla \cdot (\mu_f \nabla \mathbf{v}_a^f) = w (\mathbf{1}_s - \mathbf{1}_d), \quad (15)$$

$$\nabla \cdot \mathbf{v}_a^s = 0, \quad (16)$$

$$\nabla \cdot \mathbf{S}(\mathbf{v}_a^s) = 0. \quad (17)$$

with boundary conditions defined as

$$\begin{aligned} \mathbf{v}_a^s &= \mathbf{v}_a^f && \text{on } \Gamma_i, \\ \mathbf{S}(\mathbf{v}_a^s) \cdot \mathbf{n} &= \mathbf{T}(\mathbf{v}_a^f) \cdot \mathbf{n} && \text{on } \Gamma_i, \\ \mu_l (\nabla \mathbf{v}_a) \cdot \mathbf{n} &= -(\mathbf{v} \cdot \mathbf{n}) \mathbf{v}_a, \quad p_a = 0 && \text{on } \Gamma_n^f, \\ \mathbf{v}_a &= 0 && \text{on } \Gamma_{fd} \cup \Gamma_{sd}. \end{aligned} \quad (18)$$

It is worth noticing the duality between (18) and (7). In fact if a Dirichlet boundary condition for a state variable is set then the corresponding adjoint variable must satisfy the same type of condition in homogeneous form. The adjoint velocity \mathbf{v}_a must be continuous and different from zero on the interface since the source term $(\mathbf{1}_s - \mathbf{1}_d)$ acts in the solid

region and the information has to propagate towards the control boundary Γ_c which is part of the fluid domain. The equilibrium conditions on the interface are automatically satisfied due to the monolithic approach.

Due to the strongly non linearity and large dimensions the optimality system cannot be solved with a one-shot method, therefore in this work we use a segregate approach for the solution of the state, adjoint and gradient equations. By doing so, we can use the same solver for both the solution of the state (1-3) and adjoint systems (11-12) with minimal modifications. The simplest line search method based on a backtracking strategy is the *Steepest Descent* described in Algorithm 1. The step length r determines how

Algorithm 1 Description of the Steepest Descent algorithm.

1. Set a state $(\mathbf{v}^0, p^0, \mathbf{l}^0)$ satisfying (1-3) \triangleright *Setup of the state - Reference case*
 2. Compute the functional \mathcal{J}^0 in (8)
 3. Set $r^0 = 1$
 - for** $i = 1 \rightarrow i_{max}$ **do**
 4. Solve the system (11)-(12) to obtain the adjoint state (\mathbf{v}_a^i, p_a^i)
 5. Set the control update $\delta p^i = -(p_c^{i-1} + \mathbf{v}_a^i \cdot \mathbf{n}/\beta)$
 6. Set $r^i = r^0$
 - while** $\mathcal{J}^i(p_c^{i-1} + r^i \delta p^i) > \mathcal{J}^{i-1}(p_c^{i-1})$ **do** \triangleright *Line search*
 7. Set $r^i = \rho r^i$
 8. Solve (1-3) for the state $(\mathbf{v}^i, p^i, \mathbf{l}^i)$ with $p_c^i = p_c^{i-1} + r^i \delta p^i$
 - if** $r^i < toll$ **then**
 - Line search not successful \triangleright *End of the algorithm*
 - end if**
 - end while**
 - end for**
-

far from the current state solution we are moving along the gradient direction given by δp . Our algorithm stops either when r becomes lower than a tolerance value $toll = 10^{-6}$ or when two computed consecutive functionals are nearly identical and no more improvement is possible on the state system. It is clear that this kind of algorithm is computationally expensive, since it has to solve the state system many times for every line search, continuously reducing the step length. Furthermore this method shows a slow convergence rate since it relies only on the information available at the current iteration to determine the gradient of the functional.

The use of more sophisticated approaches, such as Newton's or quasi-Newton methods, can improve the convergence properties of the algorithm, see [11]. In fact quasi-Newton methods build an approximation of the Hessian matrix of the functional gradient using only the gradient itself at every optimization iteration. In particular, since in our work the control parameter is a scalar, the Hessian matrix denoted in the following as \mathbf{B} has to be intended as the second derivative of the functional. The control update equation

for δp becomes

$$\mathbf{B}^i = \frac{\frac{\partial \mathcal{J}}{\partial p}(p^{i-1}) - \frac{\partial \mathcal{J}}{\partial p}(p^{i-2})}{(p^{i-1} - p^{i-2})} \quad (19)$$

$$\delta p^i = -(\mathbf{B}^i)^{-1}(p_c^{i-1} + \mathbf{v}_a^i \cdot \mathbf{n}/\beta) \quad (20)$$

Clearly, since the above formula requires information from the two previous iterations, it can not be used at the beginning of the algorithm, so the first optimization iteration after the reference configuration is usually based on a steepest descent.

We implemented this algorithm in our finite element code FEMuS, which is parallelized by using openMPI libraries and uses a multigrid solver with mesh-moving capability [23, 24, 20]. We have used standard quadratic elements for all the variables except the pressure which is assumed linear to satisfy the *BBL inf-sup* condition. The displacements are approximated with standard quadratic elements as well.

3 NUMERICAL RESULTS

In this section we apply the algorithm presented to a two-dimensional channel and then to a three-dimensional geometry. For both cases we compare the results obtained with the steepest descent and quasi-Newton methods for different values of the regularization parameter β . The reference domain of our first test is shown in Figure 1 on the left. The

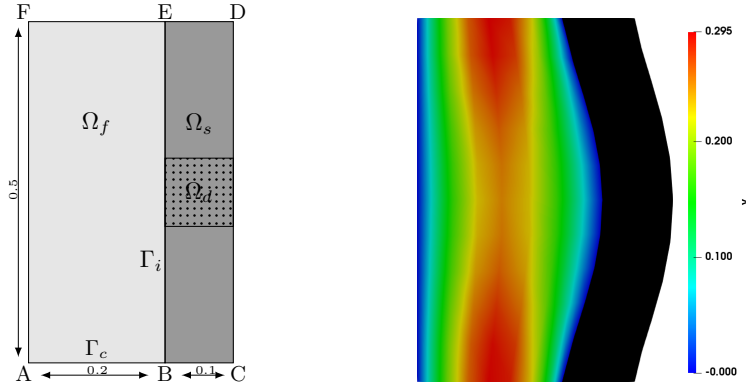


Figure 1: Left: Geometry of the channel. The dotted square on the right Ω_d is the controlled region. Right: Fluid velocity in the reference case, with no control.

region Ω_f is the fluid, Ω_s is the solid and the segment BE is the interface Γ_i . The dotted square on the right is the controlled region Ω_d . We prescribe a no-slip condition on the fluid left boundary AF . On the upper and lower fluid boundaries EF and $AB = \Gamma_c$ we impose pressure boundary conditions and vanishing tangential velocity. The pressure p_{EF} is fixed to $4 \cdot 10^3 Pa$ and $p_{AB} = 5.5 \cdot 10^3 Pa$ in the reference uncontrolled case, while $p_{AB} = p_c$ when controlling. The solid external boundary CD is left free to move, while all the others are fixed.

The physical properties are the following

$$\rho_s = \rho_f = 10^3 kg/m^3 \quad \nu_f = 0.07 m^2/s \quad \nu_s = 0.2 \quad \mu_s = 7.65 \cdot 10^4 Pa, \quad (21)$$

so that the fluid is not turbulent and the solid can easily bend. On the right of Figure 1 is reported the reference case, with no control. Here we obtain an average solid deformation along the x -component in the region Ω_d of $0.052m$. For our first test we set the target displacement to $0.07m$ thus we want to enhance the solid deformation by changing the pressure on Γ_c , in particular the control has to increase it. In Table 1 are compared the results of the optimization process obtained using both the steepest descent and quasi-Newton methods and for different values of the regularization parameter β . The results

Table 1: Effects of the regularization parameter β on objective functionals, optimization (Opt.) and line search (L.s.) number of iterations for the steepest descent and quasi-Newton methods. The reference case with no control is labeled with $\beta = \infty$.

β	Steepest descent			Quasi-Newton		
	$\mathcal{J}(\mathbf{l}, p)$	Opt.	L.s.	$\mathcal{J}(\mathbf{l}, p)$	Opt.	L.s.
∞	$9.309 \cdot 10^{-6}$	-	-	$9.309 \cdot 10^{-6}$	-	-
10^{-8}	$9.780 \cdot 10^{-8}$	10	333	$9.864 \cdot 10^{-8}$	6	39
10^{-9}	$2.743 \cdot 10^{-8}$	16	628	$2.741 \cdot 10^{-8}$	5	52
10^{-10}	$2.050 \cdot 10^{-8}$	12	552	$2.065 \cdot 10^{-8}$	6	52

show that the algorithm successfully reduces the functionals for every combination of β and method adopted. In particular for smaller values of the regularization parameter the objective term of the functional becomes larger and hence the control more accurate. Also, we notice that for a given β the two methods converge to very similar values. However the number of iterations required by the steepest descent method to converge is higher, approximately double, than that of the quasi-Newton approach and consequently a much higher number of line search iterations are performed. In Figure 2 is reported the history of the functional during the optimization iterations. Again it is worth noticing that the

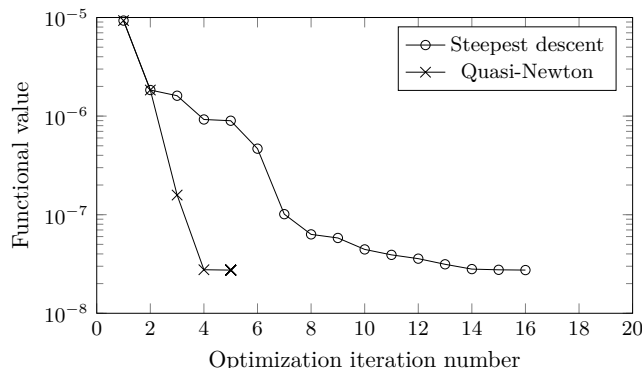


Figure 2: Convergence of the functional for the steepest descent and quasi-Newton methods, $\beta = 10^{-9}$.

quasi-Newton method converges significantly faster than the steepest descent.

3.1 Three-dimensional geometry

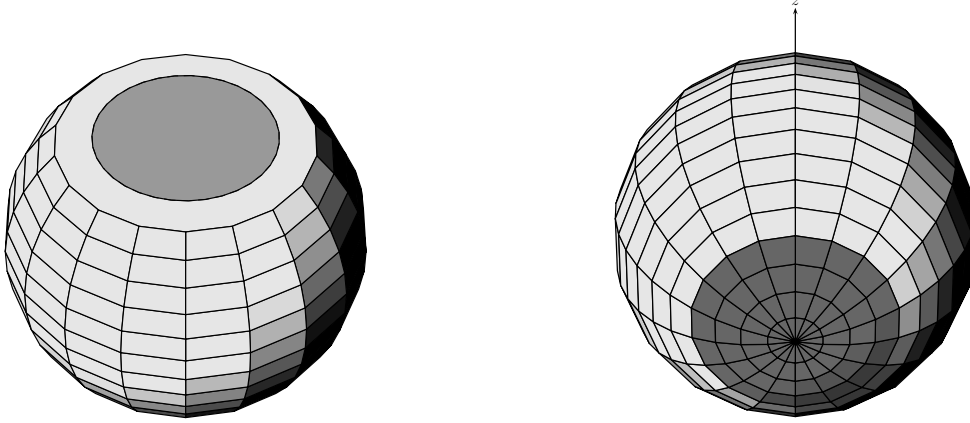


Figure 3: Case study geometry. Left: in gray is the liquid control surface Γ_c . Right: in gray is the solid controlled region Ω_d .

In this section we report the results of the three-dimensional geometry shown in Figure 3. The spherical domain consists of an external deformable solid that surrounds the internal fluid. On the upper liquid surface we prescribe a boundary condition of uniform pressure and vanishing tangential velocity while the lateral surfaces of the sphere are left free to move. Clearly by increasing the boundary pressure the solid deformation becomes more relevant. The solid and fluid properties are the following

$$\rho_s = \rho_f = 10^3 kg/m^3 \quad \nu_f = 0.02 m^2/s \quad \nu_s = 0.2 \quad \mu_s = 7.65 \cdot 10^5 Pa, \quad (22)$$

The control problem searches the optimal pressure on the upper boundary such that the z -component of the displacement over the region Ω_d shown on the right of Figure 3 matches a uniform target value. We first perform a forward simulation imposing on the inlet boundary a uniform pressure $p_{fw} = 20000 Pa$, then compute the average deformation over the controlled region and obtain $7.0982 \cdot 10^{-2} m$. This value acts as target displacement \mathbf{l}_d for our optimization test case. By doing so we expect to obtain an optimal pressure close to p_{fw} and evaluate the accuracy of our algorithm. The initial control pressure value is $p^0 = 0 Pa$, far away from the optimal one $p_{fw} = 20000 Pa$.

In Table 2 we reported the results of the optimization process obtained using both the steepest descent and quasi-Newton methods and for different values of the regularization parameter β . With p_{opt} we denoted the pressure value obtained at the end of the optimization process. We first notice that reducing β the pressure p_{opt} approaches the optimal one $p_{fw} = 20000 Pa$ since the regularization contribution of the functional becomes negligible with respect to the objective one and we obtain smaller functional values as well. The choice of the method does not afflict the accuracy of the results in terms of functional reductions and pressure values. However, focusing on a specific value of the regularization parameter, for instance 10^{-9} , the steepest descent takes 20 optimization with 126 line search iterations to converge, while the quasi-Newton takes only 5 optimization with

Table 2: Effects of the regularization parameter β on objective functionals, optimization (Opt.) and line search (L.s.) number of iterations for the steepest descent and quasi-Newton methods. The reference case with no control is labeled with $\beta = \infty$.

β	Steepest descent				Quasi-Newton			
	$\mathcal{J}(\mathbf{l}, p)$	p_{opt}	Opt.	L.s.	$\mathcal{J}(\mathbf{l}, p)$	p_{opt}	Opt.	L.s.
∞	$5.552 \cdot 10^{-5}$	0	-	-	$5.552 \cdot 10^{-5}$	0	-	-
10^{-6}	$1.223 \cdot 10^{-5}$	19 455	8	75	$1.205 \cdot 10^{-5}$	18 809	4	43
10^{-7}	$1.259 \cdot 10^{-6}$	19 959	11	88	$1.260 \cdot 10^{-6}$	19 983	6	34
10^{-8}	$1.356 \cdot 10^{-7}$	20 005	20	126	$1.355 \cdot 10^{-7}$	19 988	5	40

40 line search iterations. The latter method is then much less computationally expensive from a CPU point of view, since its implementation only requires to store some values of the functional gradient and control parameter more than for the steepest descent. Finally, in Figure 4, is reported the evolution of the functional values during the optimization process. We recall that the first iteration refers to the reference state and the second one is

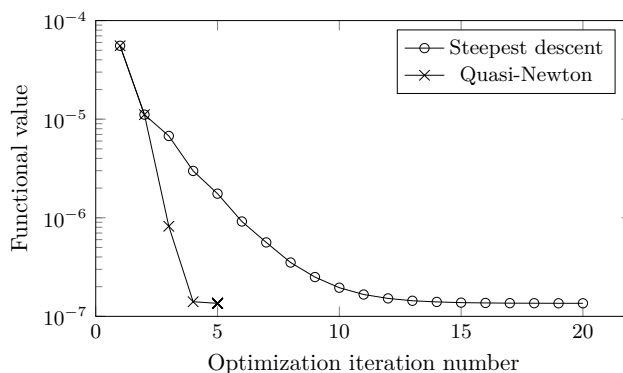


Figure 4: Convergence of the functional for the steepest descent and quasi-Newton methods, $\beta = 10^{-8}$.

always obtained with a steepest descent line search method.

4 CONCLUSIONS

In this work we have presented an optimal pressure boundary control applied to the FSI system and based on adjoint variables. The objective is the matching of a displacement field in a particular region of the solid domain by controlling the pressure on a fluid boundary. We have adopted a monolithic variational formulation to satisfy automatically the coupling conditions at the fluid-solid interface. Furthermore, we have extended the velocity field to the solid domain to couple adjoint variables and forces on the interface. The optimality system has been derived by imposing the first order necessary conditions to the full Lagrangian. The optimal solutions have been found and compared with those ones obtained by simple steepest descent algorithm and a quasi-Newton one. Both methods have shown accuracy and robustness. However we remark that the quasi-Newton

algorithm shows a faster convergence to the optimal solution. In future works we plan to assess this pressure control to more realistic geometries to show the feasibility of this optimization approach in real complex cases.

ACKNOWLEDGEMENT

The authors gratefully acknowledge the Managing Board of ECCOMAS for the scholarship covering the full registration to the Congress and the support travel and accommodation expenses.

REFERENCES

- [1] Turek S and Hron J 2006 *Fluid-structure interaction* (Springer) pp 371–385
- [2] Formaggia L, Quarteroni A and Veneziani A 2009 *Cardiovascular Mathematics, vol. 1* (Springer, Heidelberg)
- [3] Le Tallec P and Mouro J 2001 *Computer Meth. in Appl. Mech. and Eng.* **190** 3039–3067
- [4] Bukač M, Čanić S and Muha B 2015 *Journal of Computational Physics* **281** 493–517
- [5] Gilmanov A, Le T B and Sotiropoulos F 2015 *Journal of Computational Physics* **300** 814–843
- [6] Cerroni D and Manservisi S 2016 *Journal of Computational Physics* **313** 13–30
- [7] Calderer A, Kang S and Sotiropoulos F 2014 *Journal of Computational Physics* **277** 201–227
- [8] Aulisa E, Cervone A, Manservisi S and Seshaiyer P 2009 *Comm. in Comput.l Phys.* **6** 319–341
- [9] Aulisa E, Manservisi S and Seshaiyer P 2005 *Nonlinear Anal., Th., Met. and Appl.* **63** 1445–1454
- [10] Gunzburger M D 2003 *Perspectives in flow control and optimization* vol 5 (Siam)
- [11] Nocedal J and Wright S 2006 *Numerical optimization* (Springer Science & Business Media)
- [12] Rowley C W and Williams D R 2006 *Annu. Rev. Fluid Mech.* **38** 251–276
- [13] Kim J and Bewley T R 2007 *Annu. Rev. Fluid Mech.* **39** 383–417
- [14] Gunzburger M and Manservisi S 1999 *SIAM Journal on Control and Optimization* **37** 1913–1945

- [15] Gunzburger M and Manservisi S 2000 *Computer Methods in Applied Mechanics and Engineering* **189** 803–823
- [16] Maute K, Nikbay M and Farhat C 2003 *Internat. J. for Num. Meth. in Eng.* **56** 911–933
- [17] Lund E, Møller H and Jakobsen L A 2003 *Structural and Multidisciplinary Optimization* **25** 383–392
- [18] Yan Y and Keyes D E 2015 *Journal of Computational Physics* **281** 759–786
- [19] Hron J and Turek S 2006 *Fluid-structure interaction* (Springer) pp 146–170
- [20] Cerroni D, Manservisi S and Menghini F 2015 *Internat. J. of Math. Mod. and Meth. in Appl. Sci.* **9** 227–234
- [21] Adams R A 1975 *Sobolev spaces* (Academic Press, New York)
- [22] Brenner S and Scott R 2007 *The mathematical theory of finite element methods* vol 15 (Springer Science)
- [23] Aulisa E, Manservisi S and Seshaiyer P 2006 *Comput. meth. in appl. mech. and eng.* **195** 4604–4616
- [24] Bramble J H 1993 *Multigrid methods* vol 294 (CRC Press)